Princeton Plasma Physics Laboratory

PPPL-5292

Computation of Resistive Instabilities by Matched Asymptotic Expansions

Z.R. Wang and J-K Park

September 2016

PPPL PRINCETON PLASMA PHYSICS LABORATORY

Prepared for the U.S. Department of Energy under Contract DE-AC02-09CH11466.

Princeton Plasma Physics Laboratory
Report Disclaimers

Full Legal Disclaimer

Trademark Disclaimer

PPPL Report Availability

Princeton Plasma Physics Laboratory:

http://www.pppl.gov/techreports.cfm

Office of Scientific and Technical Information (OSTI):

http://www.osti.gov/scitech/

Related Links:

U.S. Department of Energy

U.S. Department of Energy Office of Science

U.S. Department of Energy Office of Fusion Energy Sciences

Computation of Resistive Instabilities by Matched Asymptotic Expansions

A. H. Glasser*
Fusion Theory and Computation, Inc., 24062 Seatter Lane NE, Kingston, WA 98346

Z. R. Wang and J.-K. Park
Princeton Plasma Physics Laboratory, P.O. Box 451, Princeton, NJ 08540
(Dated: September 12, 2016)

We present a method for determining the linear resistive magnetohydrodynamic (MHD) stability of an axisymmetric toroidal plasma, based on the method of matched asymptotic expansions. The plasma is partitioned into a set of ideal MHD outer regions, connected through resistive MHD inner regions about singular layers where $q = m/n$, with m and n toroidal mode numbers, respectively, and q the safety factor. The outer regions satisfy the ideal MHD equations with zero-frequency, which are identical to the Euler-Lagrange equations for minimizing the potential energy δW. The solutions to these equations go to infinity at the singular surfaces. The inner regions satisfy the equations of motion of resistive MHD with finite eigenvalue, resolving the singularity. Both outer and inner regions are solved numerically by newly developed singular Galerkin methods, using specialized basis functions. These solutions are matched asymptotically, providing a complex dispersion relation which is solved for global eigenvalues and eigenfunctions in full toroidal geometry. The dispersion relation may have multiple complex unstable roots, which are found by advanced root-finding methods. These methods are much faster and more robust than previous numerical methods. The new methods are applicable to more challenging high-pressure and strongly-shaped plasma equilibria and generalizable to more realistic inner region dynamics. In the thermonuclear regime, where the outer and inner regions overlap, they are also much faster and more accurate than straight-through methods, which treat the resistive MHD equations in the whole plasma volume.

PACS numbers: 52.30.Cv, 52.55.Fa

I. INTRODUCTION

The purpose of this paper is to describe numerical methods for fast and accurate determination of the resistive stability of axisymmetric toroidal plasmas by the method of matched asymptotic expansions.

In assessing the quality of a magnetically confined plasma equilibrium for magnetic fusion energy, the first criterion is to determine whether it is stable to macroscopic ideal magnetohydrodynamic (MHD) modes, since they can have high growth rates, on the order of the inverse of the Alfvén time τ_A, and can cause the plasma to rapidly degrade or disrupt. A recent paper presents a very efficient method for testing this.[1]

In ideal MHD, the field and the fluid are constrained to move together. If the equilibrium is stable to ideal modes, then in the presence of a small but finite resistivity, that constraint is relaxed, allowing the field and the fluid to slip through each other, introducing a new class of instabilities, the resistive modes, such as tearing and resistive interchange.[2–6] The main effects of resistivity and inertia are localized to the neighborhood of the singular surfaces, where $m = nq$, with m and n the poloidal and toroidal mode numbers, respectively, and q the safety factor, or winding number, of the equilibrium magnetic field. Ideal perturbations become singular at these surfaces. The singularity is resolved by allowing for finite resistivity and inertia in an inner region around the singular surface. For sufficiently high Lundquist number $S \equiv \tau_R/\tau_A \gg 1$, with τ_R the much longer resistive diffusion time, the width of the inner region is of order $S^{-1/3} \ll 1$ compared to equilibrium scale lengths, and the modes grow on a time scale of order $\tau_A S^{1/3}$, slower than ideal modes but fast compared to τ_R. This can cause rapid loss of particles and heat, as well as violent disruptions. Typical values of S in the thermonuclear regime are $10^6 - 10^9$.

This discrepancy of length and time scales is the basis for the method of matched asymptotic expansions, first introduced in Ref. [2]. The plasma domain is partitioned into a sequence of ideal MHD outer regions and resistive MHD inner regions. The outer regions are simplified by the neglect of resistivity and inertia. The inner regions are simplified by the dominance of one resonant harmonic, which reduces the dimensionality from 2 to 1 by helical symmetry. They match onto each other in a region of overlap where both approximations are well-satisfied. Coupling to a vacuum region surrounding the plasma is easily included. Matching conditions provide a dispersion relation which can be solved numerically for multiple complex eigenvalues and eigenfunctions. Computations of the inner region solutions and matching conditions are much faster than the outer region solutions and can be scanned over the parameters of the inner region at practically no cost. It is also straightforward to

*Electronic address: aglasser5@gmail.com

extend the inner region treatment to more realistic dynamics in both fluid and kinetic regimes.

The remainder of this paper is organized as follows. Section II describes the equations governing the outer ideal regions and an efficient numerical solution procedure based on an improved implementation of the singular Galerkin method introduced in Refs. [5, 6]. Section III describes the inner resistive region equations [3, 4] and an efficient new solution procedure based on another singular Galerkin method. Section IV discusses the matching conditions and dispersion relation and presents advanced methods for finding roots of the dispersion in the complex plane. Section V summarizes the results and discusses future directions. The Appendix presents dimensionless variables, scale factors, and dependent variables used in the inner region.

II. OUTER IDEAL REGIONS

In this section we describe the equations governing the outer regions and a numerical procedure for solving them to extract matching data to couple them to the inner regions.

The equations governing the outer region are the zero-frequency ideal MHD equations of motion, which are identical to the Euler-Lagrange equations for minimizing the perturbed potential energy δW. These are derived in Ref. [1] and given in Eq. (21) of that paper as

$$\mathbf{L}\boldsymbol{\Xi}(\psi) \equiv -\left(\mathbf{F}\boldsymbol{\Xi}' + \mathbf{K}\boldsymbol{\Xi}\right)' + \left(\mathbf{K}^\dagger\boldsymbol{\Xi}' + \mathbf{G}\boldsymbol{\Xi}\right) = 0, \qquad (1)$$

where $\psi \in (0,1)$ is the radial independent variable labeling flux surfaces; $\boldsymbol{\Xi}(\psi)$ is an unknown complex M-vector of Fourier amplitudes of the perturbed radial displacements; primes denote derivatives with respect to ψ; $\mathbf{F}(\psi)$, $\mathbf{K}(\psi)$, and $\mathbf{G}(\psi)$ are known complex $M \times M$ matrices that couple Fourier components and depend on equilibrium quantities; and $\mathbf{F}$ and $\mathbf{G}$ are Hermitian. Detailed expressions for $\mathbf{F}$, $\mathbf{K}$, and $\mathbf{G}$ are given in terms of equilibrium quantities in the Appendix to Ref. [1]. Equation (1) has singular points where $m = nq$, with m and n poloidal and toroidal mode numbers, respectively, and $q(\psi)$ the safety factor, or winding numer, of the equilibrium magnetic field. Power series solutions are derived in Section III of Ref. [1] for large and small resonant solutions.

In Ref. [1], devoted to ideal MHD stability, Eq. (1) is treated as a complex $2M$th-order system of ordinary differential equations in ψ, initializing $\boldsymbol{\Xi}$ to regular solutions at the magnetic axis and integrating it outward to the plasma-vacuum interface, using an adaptive ordinary differential equation (ODE) solver,[7] and using boundary conditions to cross the singular surfaces, derived from the condition that $|\delta W| < \infty$. Mathematically, this has the form of an initial value problem, even though the independent variable is ψ rather than time. Ideal stability criteria are derived from the solutions to these equations. The method is fast, accurate, and robust.

Unfortunately, attempts to adapt this numerical method to the extraction of outer region matching data for the method of matched asymptotic expansions have proven unsuccessful. The matching requirements convert the method from an initial value problem to a 2-point boundary value problem, solved by a form of shooting method, which is well-known to be numerically unstable. To avoid this, we use a different numerical method to solve Eq. (1), an improvement on the singular Galerkin method introduced in Refs. [5, 6]. Whereas the large resonant solutions must be excluded in the ideal case in order to make δW finite, it must be retained in the resistive case in order to match to the inner regions. The vector space of solutions is partitioned into a subspace for which δW is finite and a complementary subspace containing the large resonant solutions. The large resonant solutions are treated as inhomogeneities driving responses in the finite subspace. The finite subspace is expanded in a set of basis functions, converting the problem to an inhomogeneous matrix problem; see Eq. (4) beloow.

For any choice of Galerkin basis functions $\alpha_i(\psi)$, $i = 1, \ldots, n$, the unknown complex vector function $\mathbf{u}(\psi)$ in the finite subspace is expanded as

$$\mathbf{u}(\psi) = \sum_{i=1}^{n} \mathbf{u}_i \alpha_i(\psi), \qquad (2)$$

where the $\mathbf{u}_i$ are unknown amplitudes. We define the scalar product

$$(\mathbf{u}, \mathbf{v}) \equiv \int_a^b \mathbf{u}^\dagger \mathbf{v} d\psi, \qquad (3)$$

where $\mathbf{u}^\dagger$ is the Hermitian conjugate of $\mathbf{u}$ and a and b are the end-points of the ψ interval. The $\mathbf{L}$ operator is Hermitian with respect to this scalar product. To obtain the Galerkin discretization of Eq. (1), we take its scalar product with each of the basis functions $\alpha_i(\psi)$ to obtain

$$\begin{aligned} \mathbf{L}_{ij}\mathbf{u}_j \equiv \sum_{j=1}^{n} \big[&(\alpha_i', \mathbf{F}\alpha_j') + (\alpha_i', \mathbf{K}\alpha_j) \\ &+ (\alpha_i, \mathbf{K}^\dagger\alpha_j') + (\alpha_i, \mathbf{G}\alpha_j) \big] \mathbf{u}_j \\ = &-(\alpha_i, \mathbf{L}\mathbf{v}), \quad i = 1, \ldots, n, \end{aligned} \qquad (4)$$

where $\mathbf{v}(\psi)$ is an element of the complementary large resonant subspace. We have integrated the first two terms by parts and taken the boundary contributions to vanish for the case of fixed-boundary modes; see Eqs. (6) and (7) below for free-boundary modes. Each component of $\mathbf{L}_{ij}$ is a constant $M \times M$ complex matrix. If the basis functions $\alpha_i(\psi)$ have bounded support, then Eq. (4) is a complex Hermitian banded matrix equation, which can be solved efficiently with LAPACK routines ZPBTRF and ZPBTRS.[8]

The implementation of this method in the PEST III code[6] leaves room for improvement. For basis functions $\alpha_i(\psi)$, it uses linear finite elements ("tent functions")

on a noniform grid, packed to concentrate grid points in the neighborhood of the singular surfaces while leaving enough grid points to resolve the region between singular surfaces. This choice of basis functions is motivated by simplicity and completeness, which does not imply rapid convergence. The grid packing scheme is difficult to control for adequate resolution everywhere. Finally, an adequate treatment of the large resonant solutions requires evaluation of the power series in Ref. [1], Eq. (47), to high enough order to resolve the small resonant solution. The treatment of equilibrium quantities by linear interpolation does not allow for derivatives higher than first, limiting their treatment to a Mercier index $\mu = \sqrt{-D_I} \leq 1$, which can be violated by equilibria with high β and low shear q'. We have found three ways to improve on these choices, all involving better selection of basis functions.

First, we replace linear finite elements with C^1 Hermite cubics. This has two important effects: it replaces 2nd-order with 4th-order convergence; and it imposes C^1 continuity on the nonresonant harmonics, required across the singular surface to minimize the perturbed potential energy. Careful graphical examination confirms that the solutions have this property with Hermite cubics but not with linear finite elements. The role of the Hermite cubics is thus to improve the resolution of the nonresonant solutions.

Second, we improve the convergence of the outer region solutions by introducing the small resonant solution as an extra basis function in the resonant grid cells, adjacent to each singular surface. The Weierstrass convergence theorem states that polynomial approximation is uniformly convergent for functions analytic on an interval. But in the grid cells adjacent to the singular surfaces, the small and large resonant solutions vary as fractional powers of the distance from the singular surface, which are nonanalytic. To deal with this, we introduce special resonant basis functions derived from the Frobenius power series solutions. Furthermore, while all other scalar products are evaluated by Gauss-Legendre quadrature, those involving resonant basis functions are performed by adaptive integration.[7] In the solution of Eq. (4), the coefficients of the small resonant basis functions directly provide the matching data.

The layout of the grid cells in the neighborhood of a singular surface ψ_R is illustrated in Fig. 1. The Normal grid cells contain 4 Hermite cubic polynomials. The Resonant grid cells contain an additional basis function derived from the small resonant power series expansion. In the Extension grid cells, the function values and first derivatives of the small resonant basis functions are matched to the two Hermite cubic polynomials which vanish smoothly when connecting to the normal cells. The use of extra basis functions in the Resonant and Extension grid cells implies that the band width of the matrices is nonuniform, which must be taken into account in using the LAPACK routines.

Third, we use a better-controlled grid packing algorithm,

$$x(\xi,\lambda) = \frac{\tanh a\xi}{\lambda}, \quad a(\lambda) = \ln\left(\frac{1+\lambda}{1-\lambda}\right), \tag{5}$$

with $x \in (-1,1)$ the physical position of the grid cell at logical position $\xi \in (-1,1)$ and $\lambda \in (0,1)$ an adjustable parameter. The ratio of the grid density $dx/d\xi$ at $x = \pm 1$ to that at $x = 0$ is then $P(\lambda) = 1 - \lambda^2$. We control the packing algorithm by choosing $P \in (0,1)$, with $\lambda = (1-P)^{1/2}$. $P = 0$ gives a uniform grid, while $P \to 1$ gives a highly nonuniform grid, packed at ± 1. Then the interval $(-1,1)$ is linearly mapped onto the interval between singular surfaces. A suitable choice of P allows the grid to concentate near the singular surfaces while still resolving the rest of the interval. There are two extra grid cells adjacent to each side of each singular layer, called resonant and extra, whose width is adjusted separately, for the extra elements discussed above.

We note that the DCON code described in Section VI of Ref. [1] is well-suited for this problem. Equilibrium data are represented as bicubic splines in straight-fieldline coordinates ψ and θ. Their higher derivatives therefore terminate after the third one. The resonant power series solutions can be evaluated to arbitrarily high order. All of the infrastructure developed in that code is reused except one module, adaptive integration of the ideal equations, which is supplemented by the Galerkin method discussed here for resistive modes.

For fixed-boundary modes, we impose a boundary condition $\Xi(1) = 0$. For free-boundary modes, the boundary moves and perturbs the vacuum magnetic field. As in the ideal case,[1] we use the VACUUM code to compute a vacuum response matrix $\mathbf{W}_V$.[9, 10] The total energy can then be expressed as a sum of plasma and vacuum contributions,

$$\begin{aligned}\delta W =& \delta W_P + \delta W_V \\ =& \frac{1}{2}\int_0^1 d\psi \left[\Xi_\psi'^\dagger \mathbf{F} \Xi_\psi' + \Xi_\psi'^\dagger \mathbf{K} \Xi_\psi \right. \\ & \left. + \Xi_\psi^\dagger \mathbf{K}^\dagger \Xi_\psi' + \Xi_\psi^\dagger \mathbf{G} \Xi_\psi \right] + \frac{1}{2}\Xi(1)^\dagger \mathbf{W}_V \Xi(1)\end{aligned} \tag{6}$$

Then the effect of the vacuum region is to add a term to the outermost grid cell

$$\mathbf{L}_{i,j} \to \mathbf{L}_{i,j} + (\alpha_i, \mathbf{W}_V \delta(\psi - 1)\alpha_j) \tag{7}$$

This can be interpreted as an extra weight which must be moved in order to vary the boundary value of the displacement.

The discretized outer region operator $\mathbf{L}_{i,j}$ on the left-hand side of Eq. (4), with or without the free-boundary vacuum contributions in Eq. (7), is positive-definite if and only if the equilibrium is stable to ideal MHD modes. Evaluation of its lowest eigenvalues by the Lanczos method could provide an alternative to the generalized Newcomb criterion described in Ref. [1].

Since the left-hand side of Eq. (4) is positive-definite if the equilibrium is stable to ideal modes, it has no null

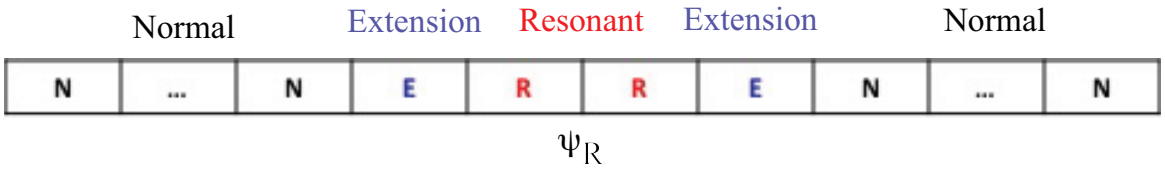

FIG. 1: Layout of Resonant, Extension, and Normal grid cells in the neighborhood of a singular surface ψ_R.

space and its inhomogeneous solutions are unique. On the right-hand side (RHS) of this equation, the M-vector $\mathbf{v}$ can be any element of the complementary subspace of large resonant solutions. To span this space, we choose a basis in which the amplitudes of all the large resonant solutions on each side of each singular surface vanish except one, whose amplitude is set to 1. Each of these basis functions drives a response in all of the small resonant solutions. By comparison, the basis chosen in Ref. [6] is formed from linear combinations of our basis functions which are even or odd about each singular surface. The scalar product on the RHS is evaluated by applying the operator $\mathbf{L}$, Eq. (1), to the large resonant power series solution derived in Section III of Ref. [1] and integrating over the resonant and extra intervals. Each inhomogeneity drives responses in all of the small resonant amplitudes on both sides of each singular surface, producing a matrix of matching data. Figure 2 illustrates the basis functions driven by large solutions to the left and right of each singular surface.

The results of this procedure can be summarized as follows. We define a set of outer region basis functions,

$$\mathbf{u}_{i,k}(\psi) \equiv \sum_{j=1}^{n}\sum_{l=L}^{R}\left[\delta_{i,j}\delta_{k,l}\mathbf{u}^{-}_{j,l}(\psi) + \Delta'_{i,k;j,l}\mathbf{u}^{+}_{j,l}(\psi)\right]. \quad (8)$$

where $i,j \in (1,n)$ label the singular surfaces, and $k,l \in \{L,R\}$ label the left and right of each singular surface, and superscript on $\mathbf{u}^{\pm}$ denotes the sign of the power given in Eq. (48) of Ref. [1]. Each basis function contains one large resonant solution $\mathbf{u}^{-}_{j,l}(\psi)$, as indicated by the Kronecker symbols $\delta_{i,j}$ and $\delta_{k,l}$. Each large resonant solution drives all of the small resonant solutions $\mathbf{u}^{+}_{j,l}(\psi)$, as indicated by the the complex coefficient matrix $\Delta'_{i,k;j,l}$, the results of the Galerkin solution. The global outer region solution is expressed as a linear combination of these basis functions,

$$\mathbf{u}(\psi) = \sum_{i=1}^{n}\sum_{k=L}^{R} c_{i,k}\mathbf{u}_{i,k}(\psi) \quad (9)$$

where the coefficients $c_{i,k}$ are determined by matching conditions to the inner region solutions, as discussed in Sections III and IV.

To verify our region singular Galerkin method, we present a Δ' benchmark between DCON code and MARS-F code [11, 12] for a tokamak with circular cross

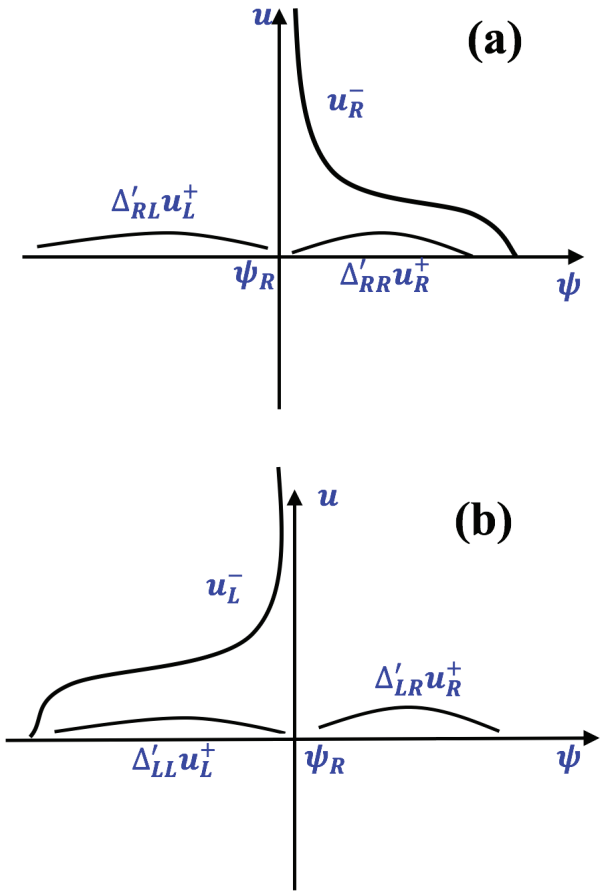

FIG. 2: Schematic drawing of the basis functions used to span the complementary subspace of large resonant solutions $\mathbf{u}^{-}_{R}$ (a) and $\mathbf{u}^{-}_{L}$ (b). Each large solution $\mathbf{u}^{-}$ drives responses in all of the small solutions $\mathbf{u}^{+}$.

section and varying aspect ratio A and the β_N value. MARS-F solves the same resistive MHD equations as DCON by a straight-through method, using the same equations everywhere without partitioning the domain. Since there is no separation between the outer and inner regions when MARS-F solves tearing instability as the eigenvalue problem, strong grid packing is required to resolve the resistive layer and to obtain a converged solution. In this benchmark, the equilibria includes only the $q = 2$ singular surface. The Δ' defined in Ref. [4–6]

is compared between DCON and MARS-F at $q = 2$ surface. The matrix $\Delta'_{i,k;j,l}$ defined in Eq. (8) can be use to express the scalar quantity Δ' as

$$\Delta' = \Delta'_{1,R;1,R} - \Delta'_{1,L;1,R} - \Delta'_{1,R;1,L} + \Delta'_{1,L;1,L} \quad (10)$$

For the straight-through method used in MARS-F, Δ' can be inferred from the separately developed inner layer model [13, 14] using the converged eigenvalue solved by MARS-F as the input. Figure 3 compares the values of Δ' solved by DCON and MARS-F, where the vacuum without the wall is included in the simulation. The comparison shows excellent agreement between the two codes over a range of values of β_N and A. We note a slight difference in the Δ' values for the case $A = 5$ because the inner layer model used by MARS-F has a large aspect ratio assumption. This does not affect the global accuracy of MARS-F because its inner region estimate is used only for comparison to DCON. The Δ' value obtained by DCON is more reliable because there is no large aspect ratio assumption.

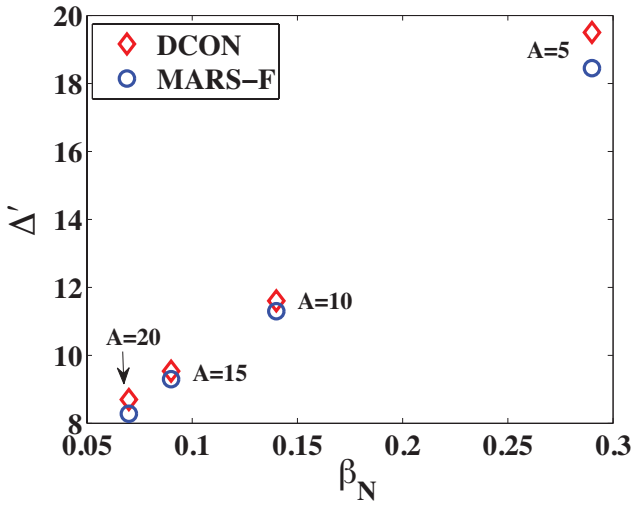

FIG. 3: Benchmark of Δ' between DCON (⋄) and MARS-F (o) at q=2 surface. A sequence of tokamak equilibria with circular cross section is used in n=1 mode simulation.

III. INNER RESISTIVE REGIONS

In this section we present a procedure for computing the inner region matching data for the resistive region equations derived in Ref. [3] from resistive MHD, using scale factors, dimensionless parameters, and dependent variables defined in the Appendix.

$$\begin{aligned}
&\Psi_{xx} - H\Upsilon_X - Q(\Psi - X\Xi) = 0,\\
&Q^2\Xi_{xx} - QX^2\Xi + QX\Psi + (E+F)\Upsilon + H\Psi_X = 0,\\
&Q\Upsilon_{xx} - X^2\Upsilon + X\Psi\\
&\quad + Q^2\left[G\left(\Xi - \Upsilon\right) - K\left(E\Xi + F\Upsilon + H\Psi_X\right)\right] = 0,
\end{aligned} \quad (11)$$

with independent variable $X \in (-\infty, \infty)$, the scaled distance from the singular surface; and eigenvalue Q, the scaled complex growth rate. The quantities E, F, G, H, and K are real, constant, dimensionless parameters characterizing the equilibrium in the neighborhood of the singular surface. The scaled dependent variable Ψ can be interpreted as either the normal component of the perturbed magnetic field or the perturbed parallel vector potential. The scaled dependent variable Ξ can be interpreted as either the normal component of the plasma displacement or the perturbed electrostatic potential. The scaled dependent variable Υ can be interpreted as either the perturbed plasma pressure or the perturbed parallel magnetic field. The first equation is the parallel component of Ohm's law, the second is the quasineutrality equation, and the third is the adiabatic pressure law. The equations are derived in Ref. [3] by a formal small parameter expansion in the resistive layer width. These dependent variables are only the resonant components, with $m = nq$ at the singular surfaces; the nonresonant components are small and ignored in the inner region. We use these equations as an example of a consistent inner region model to illustrate the method of computing inner region matching data. Later manuscripts will use the same method for more general and realistic physical models.

In Ref. [3], Eqs. (11) are solved analytically, using a subsidiary small parameter expansion with scaled growth rate $|Q| \ll 1$. In Ref. [4, 15], they are solved numerically by four different methods without a subsidiary expansion, allowing $Q \sim 1$. All of these methods fail in the limit as Q gets large, for reasons explained below. Here we derive a method which remains valid for larger values of Q, which we find to be required for realistic equilibrium conditions.

As in Ref. [4], we express these equations in matrix form,

$$\mathbf{A}\boldsymbol{\Psi}'' + \mathbf{B}\boldsymbol{\Psi}' + \mathbf{C}\boldsymbol{\Psi} = 0, \quad (12)$$

with dependent variable 3-vector

$$\boldsymbol{\Psi} \equiv \begin{pmatrix} \Psi \\ \Xi \\ \Upsilon \end{pmatrix}, \quad (13)$$

and complex 3×3 matrices

$$\mathbf{A} = \begin{pmatrix} 1 & 0 & 0 \\ 0 & Q^2 & 0 \\ 0 & 0 & Q \end{pmatrix}, \quad \mathbf{B} = \begin{pmatrix} 0 & 0 & -H \\ H & 0 & 0 \\ -KHQ^2 & 0 & 0 \end{pmatrix}, \quad (14)$$

$$\mathsf{C} = \begin{pmatrix} -Q & QX & 0 \\ QX & -Qx^2 & E+F \\ X & (G-KE)Q^2 & -X^2-(G+KF)Q^2 \end{pmatrix}. \tag{15}$$

In Appendices A and B of Ref. [4], analytical expressions are derived for the large-X behavior of the solutions of their Eq. (1), equivalent to our Eq. (12). There are two power-like solutions, which match onto the corresponding outer region solutions discussed in Section II; two exponentially large solutions, which are excluded by boundary conditions; and two exponentially small solutions, which are ignored. We present an equivalent but more compact derivation of the power-like solutions, which elucidates the nature of these solutions. The transformation matrices R and S defined below are equivalent to componentwise tranformations used in Appendix A of Ref. [4]. Then we present a new numerical procedure for solving Eq. (12) for the inner region matching conditions which requires detailed knowledge of only the power series solutions.

Before seeking a power-series solution, we balance Eq. (12) with a generalization of the shearing transformation used in Refs. [1, 4, 16], constituting a formal change of dependent variables,

$$\mathbf{\Psi} = \mathsf{R}\mathbf{u}, \quad \mathsf{R} \equiv \begin{pmatrix} X & 0 & 0 \\ 0 & 1 & 0 \\ 0 & 0 & 1 \end{pmatrix}. \tag{16}$$

followed by multiplication of Eq. 12 by a second matrix,

$$\mathsf{S} \equiv \begin{pmatrix} 1/X & 0 & 0 \\ X & 1 & 0 \\ 0 & 0 & 1/X \end{pmatrix}, \tag{17}$$

transforming it to

$$\mathsf{L}\mathbf{u} \equiv \bar{\mathsf{A}}\mathbf{u}'' + \bar{\mathsf{B}}\mathbf{u}' + \bar{\mathsf{C}}\mathbf{u} = 0, \tag{18}$$

with

$$\bar{\mathsf{A}} = \mathsf{SAR} = \begin{pmatrix} 1 & 0 & 0 \\ X^2 & Q^2 & 0 \\ 0 & 0 & Q/X^2 \end{pmatrix}, \quad \bar{\mathsf{B}} = \mathsf{S}(2\mathsf{AR}' + \mathsf{BR}) = \begin{pmatrix} 2/X & 0 & -H/X \\ (2+H)X & 0 & -HX \\ -HKQ^2/X & 0 & 0 \end{pmatrix}, \tag{19}$$

$$\bar{\mathsf{C}} = \mathsf{S}(\mathsf{AR}'' + \mathsf{BR}' + \mathsf{CR}) = \begin{pmatrix} -Q & Q & 0 \\ H & 0 & E+F \\ 1-KHQ^2/X^2 & (G-KE)Q^2/X^2 & -1-(G+KF)Q^2/X^2 \end{pmatrix}. \tag{20}$$

At large X, the coefficient matrices can be expanded as

$$\bar{\mathsf{A}} = X^2\left(\bar{\mathsf{A}}_0 + \bar{\mathsf{A}}_1 X^{-2} + \bar{\mathsf{A}}_2 X^{-4}\right), \quad \bar{\mathsf{B}} = X\left(\bar{\mathsf{B}}_0 + \bar{\mathsf{B}}_1 X^{-2}\right), \quad \bar{\mathsf{C}} = \bar{\mathsf{C}}_0 + \bar{\mathsf{C}}_1 X^{-2}. \tag{21}$$

We now seek descending power series solutions of the form

$$\mathbf{u} = X^\mu \sum_{j=0}^{\infty} X^{-2j}\mathbf{u}_j, \quad \mathbf{u}' = X^{\mu-1}\sum_{j=0}^{\infty} X^{-2j}(\mu-2j)\mathbf{u}_j, \quad \mathbf{u}'' = X^{\mu-2}\sum_{j=0}^{\infty} X^{-2j}(\mu-2j)(\mu-2j-1)\mathbf{u}_j. \tag{22}$$

Substituting Eqs. (21) and (22) into Eq. (18), we obtain

$$\begin{aligned} X^{-\mu}\mathsf{L}\mathbf{u} \equiv \sum_{j=0}^{\infty} X^{-2j}\big\{ &\left[(\mu-2j)(\mu-2j-1)\bar{\mathsf{A}}_0 + (\mu-2j)\bar{\mathsf{B}}_0 + \bar{\mathsf{C}}_0\right]\mathbf{u}_j \\ &+ \left[(\mu-2j+2)(\mu-2j+1)\bar{\mathsf{A}}_1 + (\mu-2j+2)\bar{\mathsf{B}}_1 + \bar{\mathsf{C}}_1\right]\mathbf{u}_{j-1} \\ &+ (\mu-2j+4)(\mu-2j+3)\bar{\mathsf{A}}_2\mathbf{u}_{j-2}\big\} = 0. \end{aligned} \tag{23}$$

This equation is solved order by order.

At zeroth order we obtain a matrix eigenvalue equation,

$$\mathsf{L}_0 \equiv \mu(\mu-1)\bar{\mathsf{A}}_0 + \mu\bar{\mathsf{B}}_0 + \bar{\mathsf{C}}_0, \quad \mathsf{L}_0\mathbf{u}_0 = 0. \tag{24}$$

The condition for the existence of a nontrivial solution is

$$\det \mathsf{L}_0 = Q\left(\mu^2 + \mu + E + F + H\right) = 0. \tag{25}$$

This is the indicial equation for the power μ,

$$\mu = -\frac{1}{2} \pm \sqrt{-D_I}, \quad D_I = E + F + H - \frac{1}{4}, \tag{26}$$

showing that the large-X behavior of the inner region solutions matches onto the small-x behavior of the power-like outer region solutions given in Ref. [1], Eq. (48).

The eigenvector corresponding to both values of μ, the solution to Eq. (24), is

$$\mathbf{u}_0 = \begin{pmatrix} 1 \\ 1 \\ 1 \end{pmatrix}. \tag{27}$$

The degeneracy between the two solutions is resolved at first order. Two large and two small exponential solutions could be found by multiplying Eq. (22) by exponential factors, but we do not need them.

The first-order terms in Eq. (23) give

$$\begin{aligned} \left[(\mu-2)(\mu-3)\bar{\mathbf{A}}_0 + (\mu-2)\bar{\mathbf{B}}_0 + \bar{\mathbf{C}}_0\right]\mathbf{u}_1 \\ = -\left[\mu(\mu-1)\bar{\mathbf{A}}_1 + \mu\bar{\mathbf{B}}_1 + \bar{\mathbf{C}}_1\right]\mathbf{u}_0. \end{aligned} \tag{28}$$

The properties of this equation account for a limit on the finite difference method described in Section IV of Ref. [4]. The matrix $\bar{\mathbf{C}}_1$ on the right-hand side of Eq. (28) contains the equilibrium parameters G and K multiplying the scaled growth rate factor Q^2. The small parameter ordering used in Ref. [3] treats $\beta \equiv 2\mu_0 P/B^2$ of order unity. G and K scale as $1/\beta$, getting large at low β, which is further enhanced by $Q^2 \gg 1$. In order to impose the large-X boundary conditions, excluding the exponentially large solutions and computing the inner region matching data, it is necessary to extend the numerical domain to a sufficiently large X that the zeroth order terms in Eq. (22) are larger than the first-order terms. For low β and large Q, this value of X can cause the exponentially large factor to overflow the floating point limit of IEEE double-precision arithmetic. The other methods of solution presented in Refs. [4, 15] suffer from different manifestations of the same problem.

Furthermore, these large first-order terms can broaden the inner region enough to cause a failure of overlap between the inner and outer region solutions, a prerequisite for the validity of the method of matched asymptotic expansions. While the scaling of the inner region variable $X \sim S^{-1/3}$ ensures that overlap can be achieved at sufficiently high Lundquist number S, that value of S may exceed the realistic range of S found even at thermonuclear conditions. This issue is discussed further in the next section.

We address these issues in two ways. First, we avoid the need to compute the exponential solutions by replacing the finite difference method by a finite element method, using special power-like resonant elements in the outermost grid cells, similar to our treatment of the outer region in Section II. This method remains valid to larger values of G, K, and Q than previous methods, although it eventually fails for similar reasons. Second, we monitor the overlap and exclude equilibria with sufficiently low β to cause of a failure of overlap. For such equilibria, a different inner region ordering is appropriate. Since our goal in this paper is to illustrate methods, we leave that for another effort.

For $j \geq 2$, the higher-order terms of Eq. (23) take the form of a 3-term recursion relation,

$$\begin{aligned} \left[(\mu-2j)(\mu-2j-1)\bar{\mathbf{A}}_0 + (\mu-2j)\bar{\mathbf{B}}_0 + \bar{\mathbf{C}}_0\right]\mathbf{u}_j \\ = -\big[(\mu-2j+2)(\mu-2j+1)\bar{\mathbf{A}}_1 \\ + (\mu-2j+2)\bar{\mathbf{B}}_1 + \bar{\mathbf{C}}_1\big]\mathbf{u}_{j-1} \\ - (\mu-2j+4)(\mu-2j+3)\bar{\mathbf{A}}_2\mathbf{u}_{j-2}, \end{aligned} \tag{29}$$

suitable for coding up to arbitrarily high order. The descending power series solutions in Eq. (22) are asymptotic rather than convergent; there is an optimum order, increasing with X, at which to truncate the series before the error increases with j.

The boundary conditions on Eq. (12) are that the large exponential solutions vanish for $X \to \pm\infty$. The equation has reflectional symmetry about $X = 0$. There are two independent solutions, one with even Ξ and Υ and odd Ψ, the other with odd Ξ and Υ and even Ψ. Each of these solutions contributes a quantity Δ' for matching to the outer region, as discussed in the next section. We solve for each Δ' on the half-domain $0 \leq X < \infty$, imposing even and odd boundary conditions at $X = 0$. Then we must exclude the two large exponential solutions as $X \to \infty$.

To accomplish this, we develop a variant on the singular Galerkin method used in Section II. We define a space of solutions with finite L^2 norm,

$$\int_{-\infty}^{\infty} dX |\Xi(X)|^2 < \infty. \tag{30}$$

This is satisfied by any $\Xi(X)$ excluding the exponentially large solutions and the large power-like solution, with the plus sign in Eq. (26). We expand the elements of this space in a set of basis functions,

$$\mathbf{\Psi}(X) = \sum_{j=0}^{n} \mathbf{\Psi}_j \alpha_j(X), \tag{31}$$

then take the scalar product of Eq. (12) with each basis function to obtain

$$\begin{aligned} \sum_{j=0}^{n} \left[-(\alpha_i', \mathbf{A}\alpha_j') + (\alpha_i, \mathbf{B}_j\alpha_j') + (\alpha_i, \mathbf{C}\alpha_j)\right]\mathbf{\Psi}_j \\ = -(\alpha_i, \mathbf{A}\mathbf{v}'' + \mathbf{B}\mathbf{v}' + \mathbf{C}\mathbf{v}) \end{aligned} \tag{32}$$

where we have integrated by parts on the first term, assuming the boundary terms vanish, and making use of the fact that $\mathbf{A}$ is independent of X. The right-hand side contains any element $\mathbf{v}$ of the complementary subspace containing the large resonant solution, with the plus sign in Eq. (26).

The basis functions $\alpha_i(X)$ are chosen as follows. We start with a set of C^1 Hermite cubic basis functions on

a packed grid with $0 \le X \le X_{\max}$. The grid packing algorithm for the inner region is defined by

$$X(\xi,\lambda) = \ln\left(\frac{1+\lambda\xi}{1-\lambda\xi}\right) \Big/ \ln\left(\frac{1+\lambda}{1-\lambda}\right) \qquad (33)$$

which gives a ratio of grid density at the center to that at the edge $P(\lambda) = 1-\lambda^2$. Whereas the packing algorithm defined in Eq. (5) creates a denser grid at $x = \pm 1$, this one creates a denser grid at $X = 0$. P and $X_{\max}$ are treated as adjustable parameters in a convergence study. Boundary conditions at $X = 0$ are imposed by excluding either the even or the odd basis functions in the first interval. As in the 4th-order finite difference method of Ref. [4], the Hermite cubics give 4th-order convergence.

In the last grid cell, bounded by $X_{\max}$, we replace the Hermite basis functions by the small resonant power series solution in Eq. (22), with the minus sign in Eq. (26). The large resonant solution, with the plus sign, is used to evaluate $\mathbf{v}$ on the right-hand side of Eq. (32). In the next to last grid cell, these resonant solutions are connected to Hermite cubics, which brings them smoothly to zero. The coefficients of the small resonant solution provide the inner region matching data.

Most of the scalar products on the left-hand side of Eq. (32) are evaluated by Gauss-Legendre quadrature. Those involving the descending power series solutions are non-analytic and therefore require adaptive integration with LSODE.[7]. The complex banded linear system in Eq. (32) is solved with LAPACK routines ZGBTRF and ZGBTRS.[8]

The finite-norm subspace defined by Eq. (30) contains the power-like solution with the minus sign in Eq. (26), appearing on the left-hand side of Eq. (32), while the inhomogeneity containing $\mathbf{v}$ in the complementary large subspace, is proportional to the power with the plus sign. Once this equation is discretized, we can reverse the roles of the two solutions and use the small resonant solution with the minus sign to drive a response in the large resonant solution with the plus sign. This is useful for matching to the outer region, where the plus sign denotes the small solution and the minus sign denotes to big solution, as in Eq. (8). It allows us to construct an inner region basis that more easily matches onto the outer region basis.

Figure 4 shows solutions for odd and even matching data $\Delta_\pm$ *vs.* scaled growth rate Q. This corresponds to Figure 2 of Ref. [4], but with more realistic parameters. The numerical method presented here remains accurate to $Q = 3\times 10^3$, as compared to $Q < 10$ for the methods described in Ref. [4], for the reasons explained in the discussion of Eq. (28).

As for the outer region solutions we conclude this section with a general form for the inner region solutions. We define even and odd basis functions

$$\mathbf{v}_{i,\pm}(x) \equiv \mathbf{v}^-_{i,\pm}(x) + \Delta_{i,\pm}(s)\mathbf{v}^+_{i,\pm}(x) = \pm\mathbf{v}_{i,\pm}(-x) \quad (34)$$

and construct the full inner region solution as a linear

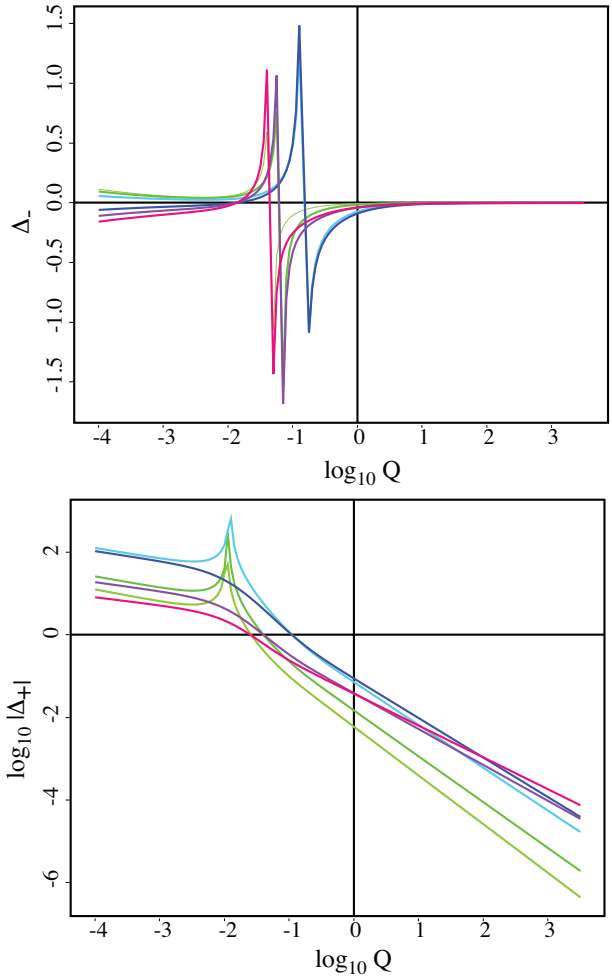

FIG. 4: Solutions for odd (top) and even (bottom) matching data $\Delta_\pm$, using parameters for the $q = 3$ surface of a D-IIID tokamak equilibrium vs. scaled growth rate Q, varying D_R from -0.1 (light green) to 0.1 (red). This is for realistic values for a D-IIID equilibrium: $F = 1.074\times10^{-6}$, $H = 1.801\times10^{-4}$, $M = 15.198$, $G = 143.9$, $K = 5.191\times10^5$.

combination of these basis functions,

$$\mathbf{v}_i(x) = d_{i,+}\mathbf{v}_{i,+}(x) + d_{i,-}\mathbf{v}_{i,-}(x) \qquad (35)$$

with the expansion coefficients $d_{i,\pm}$ determined by matching to the outer region solutions, as described in the next section.

Note that we express the basis functions and linear combination in terms of the outer region displacement x and global complex growth rate s, while the inner region equations discussed above depend on the scaled displacement X and scaled growth Q, related to the global quantities through the scale factors X_0 and Q_0 defined in Eqs. (A.14) and Eqs. (A.15). The inner region solutions are computed for each singular surface by a code DELTAC, which takes global quantities and local scale factors as input, transforms them to scaled local quantities, then returns output rescaled to global values. There

may be multiple singular surfaces, each with its own scale factors. Only the global quantities can be matched, as discussed in the next section.

The computation time required for the inner region equations is much less than for the outer region, by a factor of order 100. A key advantage of the asymptotic matching method is that the parameters of the inner region solution can be scanned over many values, for root-finding and varying physical conditions, without recomputing the outer region solution.

IV. MATCHING CONDITIONS

In Section II, we describe a procedure for accurately computing the outer region matching data, culminating in Eqs. (8) and (9). In Section III, we present a procedure for accurately computing the inner region matching data, culminating in Eqs. (34) and (35). In this section, we show how to use these matching data to assemble a global solution, we derive a dispersion relation for the global complex growth rate, and we describe numerical procedures for finding roots of this dispersion relation.

On each side of each singular surface, the plus and minus inner and outer region solutions must match onto each other. The matching conditions for the minus solutions on the left and right of the jth singular surface are

$$c_{j,L} = d_{j,+} - d_{j,-}, \quad c_{j,R} = d_{j,+} + d_{j,-} \tag{36}$$

while the matching conditions for plus solutions on the left and the right are

$$\begin{aligned} \sum_{i=1}^{n} \sum_{k=L}^{R} c_{i,k} \Delta'_{i,k;j,L} =& d_{j,+} \Delta_{j,+}(s) - d_{j,-} \Delta_{j,-}(s) \\ \sum_{i=1}^{n} \sum_{k=L}^{R} c_{i,k} \Delta'_{i,k;j,R} =& d_{j,+} \Delta_{j,+}(s) + d_{j,-} \Delta_{j,-}(s), \end{aligned} \tag{37}$$

where we note that the inner region quantities depend upon the global complex growth rate while the outer region quantities do not.

These matching conditions can be expressed in matrix form. We define a column $2n$-vector $\mathbf{c}$ of all the unknown expansion coefficients,

$$\mathbf{c} \equiv (c_{1L}, d_{1+}, d_{1-}, c_{1R}, \cdots, c_{nL}, d_{n+}, d_{n-}, c_{nR})^T. \tag{38}$$

Then the matching conditions, Eqs. (36) and (37) can be combined into a homogeneous matrix equation,

$$\mathbf{M}(s)\mathbf{c} = 0. \tag{39}$$

The condition for the existence of a nontrivial solution is then the global dispersion relation

$$\det \mathbf{M}(s) = 0, \tag{40}$$

where s is the complex growth rate.

There is an important point to note about requirements for overlap of the inner and outer region solutions, as discussed in the previous section. Both the outer region power series, given in Ref. [1], Section III, and the inner region power series, given in Eq. (22) *et seq.* of this paper, can be carried to high order, which accelerates convergence of the matching data. But the higher-order terms in the two power series represent different physics. The outer region equations contain only ideal MHD, but more complex geometry, including nonresonant terms. The inner region equations treat only the resonant terms but include inertial and resistive effects as well as ideal MHD. Matching occurs only for the zeroth-order terms of both power series, which vary with the same powers of the distance x from the singular surface. In order for the matching method to be valid, there must be a region of overlap where both the inner and outer region solutions are well-represented by the zeroth-order terms in their respective power series. Because the inner region scale factor X_0, Eq. (A.15), scales as $S^{-1/3}$, there is always a regime of adequate overlap for large enough S, but this can require values of S even larger than in thermonuclear plasmas. It is important to monitor the overlap in order to know when it is sufficient.

Equation (40) requires that we find the complex roots of a complex function. Roots in the complex half-plane $\Re s > 0$ represent instabilities. Once a root has been found, the corresponding eigenfunction can be computed as a solution to Eq. (39). There may be multiple roots with different growth rates and eigenfunctions. It is important to find all unstable roots. While the most unstable root, with the largest growth rate $\Re s$, may be the most important, other roots with smaller growth rates may also play a role in the nonlinear evolution of the plasma, which is beyond the scope of this paper. It should be noted that this procedure is also capable of finding stable roots.

We use two numerical methods to locate roots. If we can find a good initial iterate s_0, sufficiently close to a root, then we can use a complex secant method to locate the root. Once a root s_0 has been found, then we can search for other roots by using deflation. The dispersion function $\det M(s)$ is divided by $s - s_0$, effectively removing that root and allowing the secant iteration to search elsewhere.

A second method uses a generalization of the Nyquist method described in Ref. [3]. A contour in the complex s plane is defined which encircles the unstable half plane, avoiding poles at 0 and ∞. The image of this contour is then plotted in the complex $\det M$ plane. The number of times the image contour encircles the origin is the number of zeroes minus the number of poles. The generalization is that the innermost and outermost semicircles of the s contour may be varied over a range of values, allowing better localization of the roots and poles. The results of this procedure can then be used as initial iterates for the first procedure.

The solutions in the outer and inner regions are

matched with the matching matrix **M**. Figure 5 illustrates how the resonant harmonic of the perturbed radial displacement matches between the outer and inner regions at the $q = 2$ surface. The equilibrium used in this simulation has $q_0 = 1.05$, $q_a = 2.31$, $\beta_N = 0.77$, and $A = 2.73$, with the $q = 2$ surface located at $\psi = 0.94766$. Figure 5 shows good overlap between the inner and outer region solutions where both solutions are valid.

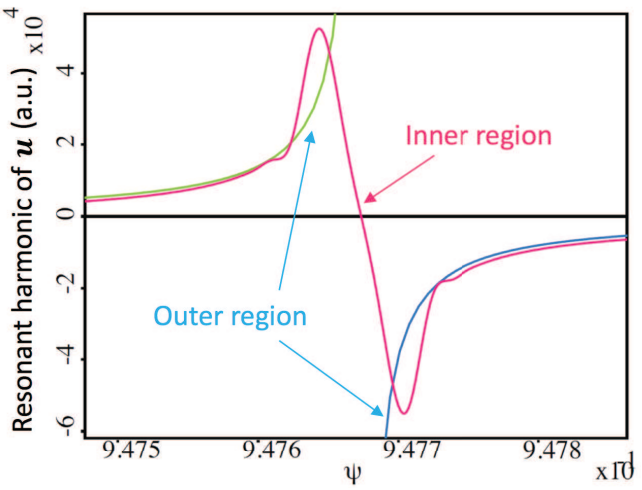

FIG. 5: Schematic of solution overlap between the outer and inner regions. The resonant harmonic of perturbed radial displacement **u** is plotted for both outer and inner regions respectively.

A comparison of growth rate γ between DCON and MARS-F for the $n = 1$ tearing mode is shown in figure 6. The equilibrium used in this comparison is the same as in figure 5. This shows a very good quantitative agreement of growth rate for both real and imaginary parts. With increasing Lundquist number S, both codes indicate that the mode approaches marginal stability. Note that the narrower resistive layer at high S is more difficult to resolve in MARS-F, which solves the resistive MHD equation in whole plasma volume and relies on grid packing for resolution. Since DCON only needs to solve the outer region once and the inner layer computation is much faster, this greatly reduces the computational effort required for DCON, allowing for very efficient parameter scans with fine resolution, as shown in figure 6. Therefore, DCON is very useful to explore parameter space for the tearing instability. This is indicated in the figure by the much larger number of points for DCON than for MARS-F.

A forthcoming manuscript will present more extensive verification against the MARS-F code for a wider variety of equilibria.

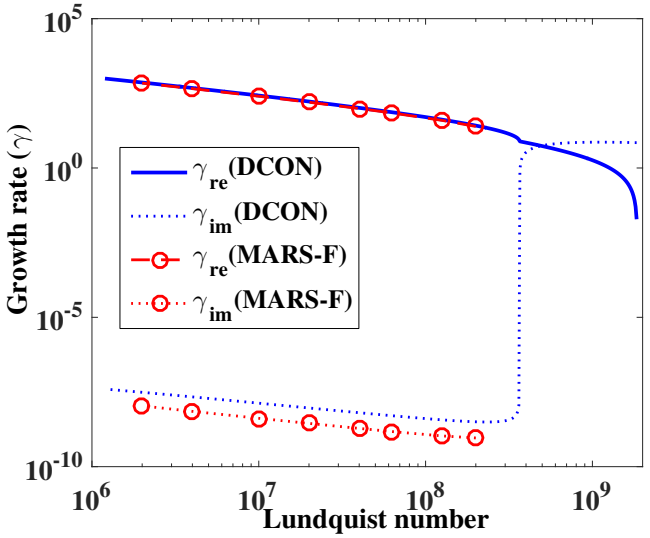

FIG. 6: Comparison of growth rates between DCON and MARS-F ('o'). The real and imaginary parts of growth rate are presented by the solid line and the doted line respectively, where the equilibrium with $q_0 = 1.05, q_a = 2.31, \beta_N = 0.77$ and $A = 2.73$ is used in the simulation.

V. DISCUSSION AND CONCLUSIONS

We have presented a procedure based on the method of matched asymptotic expansions for determining the resistive stability of axisymmetric toroidal plasmas. A singular Galerkin method is developed for solution of the ideal MHD marginal equations, the Euler-Lagrange equations for minimizing the energy δW, provides outer region matching data. Another singular Galerkin method applied to the inner region equations of Ref. [3] provides inner matching data for each of the singular surfaces in the plasma. The inner and outer matching data are combined into a dispersion relation, which is solved by complex root-finding methods. This method provides very fast and accurate solutions for realistic equilibria in the regime of large Lundquist number S.

It is essential to verify the results of this procedure against results obtained by straight-through methods, such as the MARS code. [17] This will be the subject of another manuscript.

Two publications [15, 18] solve the outer and inner region problems, respectively, by extracting the leading-order power of the large resonant solution from the resonant displacement prior to solving for the remaining factors numerically. This method is related to the singular Galerkin method used here, but with important differences. We use both the large and small resonant solutions to high order as extra Galerkin basis functions, rather than extracting the leading-order power as a factor. For Mercier index $\mu > 1$, higher-order terms in the large resonant power series are required to accurately compute the small resonant solution. Furthermore, even

after extraction of the leading fractional power, the remaining functions are non-analytic in the neighborhood of the singular point, and therefore subject to the Weierstrass approximation theorem discussed in section II. A detailed comparison between our methods and those of Refs. [15, 18] is beyond the scope of this paper.

The methods presented here use simple resistive MHD to model the inner region. A more complete fluid model of the inner region can include many additional terms in the Braginskii fluid equations,[19] such as anisotropic viscosity, thermal conductivity, electrical conductivity, and sheared equilibrium rotation, appropriate for the regime of short mean free path. In the regime of long mean free path, equations for linear neoclassical tearing modes have been derived.[20] All of these treatments are amenable to the inner region singular Galerkin method developed in Section III. They will be the subjects of future manuscripts.

Acknowledgments

The authors acknowledge helpful discussions with Jon Menard, Steve Jardin, Dylan Brennan, and Yueqiang Lui.

This work was supported by the following contracts from the U.S. Department of Energy, Office of Fusion Energy Sciences: DE-FG02-05ER54811, DE-AC02-09CH11466, and DE-SC0016106.

Appendix: Dimensionless Parameters, Scale Factors, and Dependent Variables

In this appendix we give expressions for inner region dimensionless parameters, scale factors, and dependent variables local to each singular layer. These expressions are equivalent to those defined in Ref. [3], but are given here in terms of more current notation and for arbitrary straight-fieldline coordinate systems.

The equilibrium magnetic field is given in two forms, in standard axisymmetric form,

$$\mathbf{B} = f\nabla\phi + \chi'(\psi)\nabla\phi\times\nabla\psi, \tag{A.1}$$

where ϕ is the polar angle about the axis of symmetry, and in terms of straight-fieldline coordinates

$$\mathbf{B} = \chi'(\psi)[\nabla\zeta - q(\psi)\nabla\theta]\times\nabla\psi, \tag{A.2}$$

where the specification that q is a function of ψ only is the defining feature of straight-fieldline coordinates ψ,θ,ζ, where θ and ζ increase by 2π in going around the short way and the long way, respectively, with the radial variable ψ labeling flux surfaces and normalized to go from 0 at the magnetic axis to 1 at the plasma-vacuum interface. Primes denote derivatives with respect to ψ. The Jacobian of the coordinate system is given by

$$\mathcal{J}(\psi,\theta) \equiv (\nabla\psi\times\nabla\theta\cdot\nabla\zeta)^{-1}. \tag{A.3}$$

The integral of $\mathcal{J}$ over a flux surface is given by

$$\oint d\theta \oint d\zeta \mathcal{J}(\psi,\theta) = V'(\psi), \tag{A.4}$$

where $V(\psi)$ is the volume enclosed within a flux surface. The equilibrium pressure $P(\psi)$ is isotropic and constant along the magnetic field. The equilibrium current satisfies $\mu_0\mathbf{J} = \nabla\times\mathbf{B}$ and $\mathbf{J}\times\mathbf{B} = \nabla P$, which yields the Grad-Shafranov equation,

$$\Delta^*\chi \equiv R^2\nabla\cdot\left(\frac{1}{R^2}\nabla\chi\right) = -\frac{4\pi^2}{\chi'}(ff' + \mu_0R^2P') \tag{A.5}$$

A singular surface at $\psi = \psi_0$ satisfies the truncated Taylor expansion

$$q(\psi) = q_0 + q_0'(\psi-\psi_0) + \cdots, \tag{A.6}$$

with $q_0 = m/n$, m and n integers, and $q_0' \neq 0$. The fieldline average of any function $\mathcal{F}(\psi,\theta)$ over the singular surface is defined by

$$\langle\mathcal{F}\rangle \equiv \frac{\oint \mathcal{F}(\psi,\theta)\mathcal{J}(\psi,\theta)d\theta}{\oint \mathcal{J}(\psi,\theta)d\theta}. \tag{A.7}$$

The following dimensionless parameters are used in Eq. (11) and elsewhere:

$$\begin{aligned}
E \equiv& \frac{P'V'}{\left(4\pi^2\chi'^2q_0'\right)^2}\left\langle\frac{B^2}{|\nabla\psi|^2}\right\rangle\left(\frac{4\pi^2\chi'q_0'f}{\langle B^2\rangle} + \frac{\chi''V' - V''\chi'}{\chi'}\right),\\
F \equiv& \left(\frac{P'V'^2}{4\pi^2\chi'^2q_0'}\right)^2\left\langle\frac{B^2}{|\nabla\psi|^2}\right\rangle\\
&\times\left[\left\langle\frac{1}{B^2}\right\rangle + \left(\frac{f}{\chi'}\right)^2\left(\left\langle\frac{1}{B^2|\nabla\psi|^2}\right\rangle - \frac{\left\langle 1/|\nabla\psi|^2\right\rangle^2}{\langle B^2/|\nabla\psi|^2\rangle}\right)\right],\\
H \equiv& \frac{P'V'f}{4\pi^2\chi'^3q_0'}\left\langle\frac{B^2}{|\nabla\psi|^2}\right\rangle\left(\frac{\left\langle 1/|\nabla\psi|^2\right\rangle}{\langle B^2/|\nabla\psi|^2\rangle} - \frac{1}{\langle B^2\rangle}\right),\\
M \equiv& \left\langle\frac{B^2}{|\nabla\psi|^2}\right\rangle\left[\left\langle\frac{|\nabla\psi|^2}{B^2}\right\rangle + \left(\frac{f}{\chi'}\right)^2\left(\left\langle\frac{1}{B^2}\right\rangle - \frac{1}{\langle B^2\rangle}\right)\right],\\
G \equiv& \frac{\langle B^2\rangle}{M\gamma P}, \qquad K \equiv \left(\frac{4\pi^2\chi'^2q_0'}{P'V'}\right)^2\frac{\langle B^2\rangle}{M\left\langle B^2/|\nabla\psi|^2\right\rangle},
\end{aligned} \tag{A.8}$$

with F, G, K, and M positive-definite. There are two important quantities derived from these parameters:

$$D_I \equiv E + F + H - 1/4, \tag{A.9}$$

which occurs in the power-like behavior defined in Eq. (26) and indicates local ideal Mercier interchange instability for $D_I > 0$;[1] and

$$D_R \equiv E + F + H^2 = D_I + (H - 1/2)^2, \tag{A.10}$$

which indicates local resistive interchange instability for $D_R > 0$.[3]

To express the inner region equations in dimensionless form, we define scale factors X_0 for displacement and Q_0 for growth rate. Let $x \equiv \psi - \psi_0$ be the displacement from the singular surface in the radial flux coordinate and let s be the complex growth rate. Then we define

$$x = X_0 X, \quad s = Q_0 Q \tag{A.11}$$

with X the dimensionless scaled distance from the singular surface and Q a dimensionless growth rate, both scaled to the behavior of the resistive interchange. The scale factors satisfy two equations characterizing the mode: a diffusive scaling law

$$Q_0 X_0^2 = \frac{\eta \langle B^2 \rangle}{\langle B^2/|\nabla\psi|^2\rangle} \equiv \frac{1}{\tau_R}; \tag{A.12}$$

with ρ the plasma mass density, and an inertial scaling law

$$\frac{Q_0^2}{X_0^2} = \frac{1}{\rho M}\left(\frac{4\pi^2 n\chi' q_0'}{V'}\right)^2 \equiv \frac{1}{\tau_A^2}. \tag{A.13}$$

with η the plasma resistivity. From these we obtain the following expressions,

$$Q_0 = \left(\frac{\eta \langle B^2 \rangle}{\langle B^2/|\nabla\psi|^2\rangle}\right)^{1/3}\left[\frac{1}{\rho M}\left(\frac{4\pi^2 n\chi' q'}{V'}\right)^2\right]^{1/3}, \tag{A.14}$$

$$X_0 = \left(\frac{\eta \langle B^2 \rangle}{\langle B^2/|\nabla\psi|^2\rangle}\right)^{1/3}\left[\frac{1}{\rho M}\left(\frac{4\pi^2 n\chi' q'}{V'}\right)^2\right]^{-1/6}. \tag{A.15}$$

Then we define the local Lundquist number

$$S \equiv \frac{\tau_R}{\tau_A} \gg 1, \quad Q_0 \tau_A = X_0 = S^{-1/3} \ll 1. \tag{A.16}$$

Finally, we define the three dimensionless dependent variables used in Eq. (11), in two equivalent ways, the first corresponding to the definitions in Ref. [3], the second in a representation that uses electrostatic potential φ and vector potential $\mathbf{A}$,

$$\begin{aligned}
\Psi \equiv & \frac{V'}{4\pi^2 i n\chi' q_0' X_0}\langle \mathbf{b}\cdot\nabla\psi\rangle^{(1)} \\
= & -\frac{V'}{4\pi^2\chi' q_0' X_0}\langle \mathbf{A}\cdot(\nabla\zeta - q_0\nabla\theta)\times\nabla\psi\rangle^{(1)}, \\
\Xi \equiv & \langle \boldsymbol{\xi}\cdot\nabla\psi\rangle^{(0)} = -\frac{in}{s\chi'}\varphi^{(1)}, \\
\Upsilon \equiv & \frac{\langle \mathbf{b}\cdot\mathbf{B}\rangle^{(0)}}{P'} = -\frac{p^{(0)}}{P'}.
\end{aligned} \tag{A.17}$$

[1] A. H. Glasser, Phys. Plasmas **23**, 072505 (2016).
[2] H. P. Furth, J. Killeen, and M. N. Rosenbluth, Phys. Fluids **6**, 459 (1963).
[3] A. H. Glasser, J. M. Greene, and J. L. Johnson, Phys. Fluids **18**, 875 (1975).
[4] A. Glasser, S. Jardin, and G. Tesauro, Phys. Fluids **27**, 1225 (1984).
[5] R. L. Dewar and A. Pletzer, J. Plasma Physics **43**, 291 (1990).
[6] A. Pletzer, A. Bondeson, and R. L. Dewar, J. Comp. Phys. **15**, 530 (1994).
[7] A. Hindmarsh, in *Scientific Computing*, edited by R. Stepleman (North-Holland, Amsterdam, 1983).
[8] E. Anderson, Z. Bai, C. Bischof, S. Blackford, J. Demmel, J. Dongarra, J. Du Croz, A. Greenbaum, S. Hammarling, A. McKenney, et al., *LAPACK User's Guide* (Society for Industrial and Applied Mathematics, Philadelphia, PA, 1999), 3rd ed.
[9] M. Chance, Phys. Plasmas **4**, 2161 (1997).
[10] M. Chance, A. Turnbull, and P. Snyder, J. Comp. Phys. **221**, 330 (20066).
[11] Y. Liu, A. Bondeson, C. Fransson, B. Lennartson, and C. Breitholtz, Phys. Plasmas **7**, 3681 (2000).
[12] Y. Liu, A. Kirk, and E. Nardon, Phy. Plasmas (2010).
[13] Y. Liu, R. Hastie, and T. Hender, Phys. Plasmas **19**, 092510 (2012).
[14] A. Glasser, J. Greene, and J. Johnson, Phys. Fluids **19**, 567 (1976).
[15] S. Galkin, A. Turnbull, J. Greene, and M. Chu, Phys. Plasmas **7**, 4070 (2000).
[16] H. Turrittin, Acta Mathematica **93**, 27 (1955).
[17] D. H. Liu and A. Bondeson, Comp. Phys. Comm **116**, 55 (1999).
[18] S. Galkin, A. Turnbull, J. Greene, and D. Brennan, Phys. Plasmas **9**, 3969 (2002).
[19] S. I. Braginskii, *Reviewes of Plasma Physics* (Consultants Bureau, New York, 1965), vol. 1, p. 205.
[20] J. W. Connor, R. J. Hastie, and P. Helander, Plasma Phys. Control. Fusion **51**, 015009 (2009).

PPPL PRINCETON PLASMA PHYSICS LABORATORY

Princeton Plasma Physics Laboratory
Office of Reports and Publications

Managed by
Princeton University

under contract with the
U.S. Department of Energy
(DE-AC02-09CH11466)

P.O. Box 451, Princeton, NJ 08543
Phone: 609-243-2245
Fax: 609-243-2751

E-mail: publications@pppl.gov

Website: http://www.pppl.gov